Chapter VIII. Computational modeling in the edge plasma studies

Given the broad variety of the physical processes occurring in the edge plasma on very different time scales, it would be impractical to attempt producing a single, comprehensive model describing all the processes in the plasma edge from the first principles. Due to the large disparity of the characteristic time and length scales involved, such a model would require computer resources orders of magnitude larger than available at present or in the near future. Moreover, even if such a model were developed, it would probably require a special theory describing the detail of the model itself and the "second-order" modeling of the processes involved in order to understand the results. Most of the collision processes involving the edge plasma and neutral gas species occur on sub-microsecond time scales. The small-scale turbulence develops in a fraction of a millisecond. The time scale of equilibration of the plasma parameters along the magnetic field is determined by the sound speed and connection length and is typically several tens milliseconds, which is also the time scale for the cross-field transport outside the separatrix. Finally, the evolution of the state of the material surfaces surrounding the plasma, which determines the recycling conditions and impurity production rate, can take 100's to 1000's seconds until the saturation (if any) is achieved. Therefore, there is a more than nine orders of magnitude span of the time scales involved in the physical processes in the edge plasma, so resolving all of them in one model looks unrealistic.

The equations describing the edge plasma are very complex, so analytical treatment is only possible with introducing strong simplifying assumptions that are not always strictly justified. The experimental data are difficult to obtain and the measurements are not straightforward to interpret. Therefore, one needs a bridge between the theoretical understanding and experimental observations and this bridge is offered by computational modeling.

Today one can identify two main directions in the edge plasma modeling. One of them focuses on fast, relatively small-scale plasma instabilities and turbulence, which govern anomalous cross-field plasma transport (see Ch. VII for further discussions). The other one is aimed at characterizing the large spatiotemporal scale quasi-equilibria and flows of particles and energy in complex divertor geometries, including coupling to neutrals, sheath boundaries, atomic physics, plasma-surface interactions, etc. The codes used for this second direction, the so-called "edge plasma transport codes", include the effects of small-scale fluctuations by using some "anomalous" transport coefficients. These coefficients could be provided by the plasma turbulence codes, but most often, they are obtained by fitting the results of experimental measurements in the edge plasma. In this chapter, we discuss the main approaches to the edge plasma modeling with the transport codes.

Generally, the edge plasma of a tokamak or, especially, a stellarator is a 3D object. Correspondingly, a 3D transport model would be desirable. However, even in the transport approximation, a full 3D model becomes too complex and its numerical realization is too slow for practical use. Therefore, 2D and even 1D plasma transport codes are typically used for the interpretation of experimental results and comparison with theoretical models [1]. There is significant progress in the development of the 3D codes [2] oriented primarily to the description of the plasma edge in stellarators where the toroidal symmetry approximation is not applicable. However, we focus here on the 2D transport models since they are most developed and widely used for tokamak modeling.

VIII.1. Transport modeling of the plasma

In the edge plasma, where the flow patterns that determine the distribution of the plasma parameters and wall loading form, the neutral particles, such as atoms and molecules, are abundant and play an important role in the physical processes occurring there. Since the neutrals, unlike the charged plasma particles, are not magnetized, their description may require a different approach. If the distribution functions of the plasma components are not far from Maxwellian (the assumption used in the transport models), then the plasma state is characterized by the density, fluid velocity and temperature of all sorts of the charged particles involved in the model. The spatial profiles of these quantities and their time evolution are described with a set of equations for the particle and energy densities and parallel momentum of the different plasma species. Different forms of such transport equations are used in different codes (see Ch. VI). One of the forms of these equations is

$$\frac{\partial U_s}{\partial t} + \nabla \cdot \vec{\Gamma}_{U_s} = S_{U_s}, \qquad \text{(VIII.1)}$$

where U_s corresponds to the particle and energy densities and parallel momentum of the species s, whereas $\vec{\Gamma}_{U_s}$ and S_{U_s} describe the flux of these quantities and the effective "source" terms which cannot be written in the form of divergence (e.g. the sink/source of the particles, the friction force, etc.).

Since the plasma is magnetized and the modeling is aimed at resolution of the effects occurring on a time scale much longer than the ion gyration time, the momentum component parallel to the magnetic field is only retained in the momentum equations and a simplified description of the perpendicular flux components (usually, the diffusive approximation) is used in all the equations. Due to the mass difference, temperature relaxation between different sorts of ions is much faster than between the ions and electrons, so the energy transport equations for all the sorts of ions are often combined in one equation, assuming the common temperature T_i for all the ions. Because of small electron mass and plasma quasi-neutrality, no separate electron parallel momentums and continuity equations are used.

The electric field, which develops in the edge plasma, is described by the equation (V.52), which is derived from the condition of zero divergence of the electric current. The principal sources for these currents are the electron and ion magnetic drifts and anomalous cross-field plasma transport, as well as the difference in the sheath potential at the two targets connected by the magnetic field lines. Plasma transport in a strong magnetic field is anisotropic. It is fast along the magnetic field and relatively slow, by diffusion or intermittent convection, across (see Ch. VII). Correspondingly, the coordinate system used for the representation of Eq. (VIII.1) in modeling is usually aligned with the magnetic field. This helps one to avoid "contamination" of the weak cross-field transport terms with the strong parallel transport by discretization of the equations.

VIII.1.1. Model geometry

In the toroidal symmetry approximation, the 2D model geometry is represented with a radial cross-section of the tokamak (the poloidal plane), Fig. VIII.1. The computational grid for the plasma transport description is aligned with the magnetic surfaces and the flows parallel or normal to the magnetic field lines are projected onto the poloidal plane, thus translating the anisotropy with respect to the magnetic field into anisotropy with respect to the magnetic surfaces and making the problem two-dimensional. The shape of the grid reflects the magnetic

field topology, see the example in Fig. VIII.1. In most major codes, such as EDGE2D [3], SOLPS [4] and UEDGE [5], the radial extent of the grid is limited by the first intersection with a material surface other than a target. This allows projection of the curvilinear grid onto a topologically equivalent, rectangular one, Fig. VIII.1, and simplifies coding. In the equations written on the rectangular grid, the real geometry is included through the metric coefficients and the transport anisotropy appears distinctly in the boundary conditions. For a single-null divertor configuration, there are two sides of the rectangle corresponding to the targets and two others where the plasma fluxes only have the component normal to the magnetic field. This simplification can be justified for modeling plasma interaction with the targets since most of the power going through the SOL is concentrated in a narrow layer just outside the separatrix [6], [7], which is not strongly affected by interaction with the side walls. However, when the plasma profiles near, or fluxes onto the sidewall come into question, the grid needs to be extended to cover the whole chamber. Grids of this kind are implemented in the SOLEDGE2D-Eirene [8] and SOLPS [9] code packages, but they are not used widely yet.

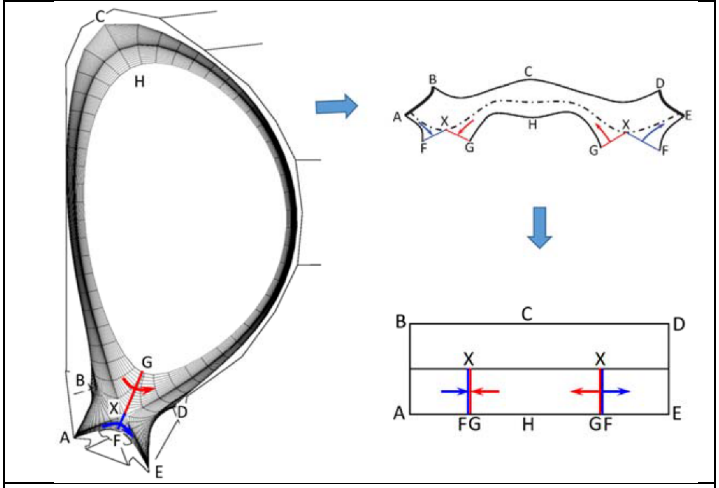

Fig. VIII.1. Typical grid used for discretization of the edge plasma transport equations and the topologically equivalent rectangular grid. Arrows indicate correspondence between the fluxes on the grid cuts. The grid transformation can be presented as (a) cutting the grid along the FG line, (b) unfolding it and (c) distorting it to make rectangular, hiding the curvilinearity in the metric coefficients in the equations. Reproduced with permission from [10], © Cambridge University Press 2017.

VIII.1.2. Parallel transport

Plasma transport along the magnetic field is usually described with Braginckii-type [11] terms which are valid if the ratio, γ, of the Coulomb mean-free path λ_C of the charged particles to the scale length L of variation of the plasma parameters along the field line is small. However, the validity of the expressions for the high order moments of the distribution functions, e.g. those describing the heat fluxes [12], requires this parameter to be really small, $\gamma < 10^{-2}$ (see e.g. [13], [14]), which in practice does not hold. At the values of $\gamma > 10^{-2}$, which is the typical situation in the SOL plasma, the heat is mostly transported by supra-thermal particles having a longer mean-free path and the parallel energy transport becomes non-local – the flux is determined by the whole temperature profile, not by the local values of the plasma parameters and their gradients. Physically, this means that the hot tails of the distribution functions are depleted in the hot SOL and enhanced in the colder divertor region, therefore reducing the heat flux upstream (see section VI.4 for details). The empirical way of taking this reduction of the conducted energy flux into account is the introduction of the so-called flux-limit factors that effectively limit the conducted flux to some fraction of the free-streaming one, see Eq. (V.42). As noted in Ch. VI, this approach describes reasonably well the reduction of the heat flux upstream because of the depletion of the hot tails of the distribution functions there but does not take into account the appearance of these supra-thermal particles in the cold plasma. This may be

not so important since, in the divertor regions, where intensive particle recycling occurs, the heat fluxes are dominated by convective transport [12]. In addition, low electron temperature and high plasma density in the recycling region cause strong dissipation of the electron tail so that it does not affect the ionization rates strongly [13]. The heat flux correction with the flux limiting factors is implemented in virtually all major 2D modeling codes together with similar treatment of the parallel viscosity coefficient.

In principle, non-local transport requires a full kinetic description that allows a significant deviation of the velocity distribution functions of the charged particles from the Maxwellian ones. However, full kinetic treatment of a problem including many different interactions occurring on different time scales with adequate spatial resolution does not look realistic at the present state of computer development. Given the complexity of the full kinetic treatment, the attempts have been made to combine a simplified kinetic model with a fluid model of the edge plasma, treating the Coulomb collisions in kinetics and leaving the slower processes for the fluid description. In [12], a simplified kinetic model in the BGK approximation [14] was combined with a 2D fluid model. The solution was obtained in iterations where the plasma parameters from the fluid model were taken as the background for the kinetic calculations for electrons and ions, then the effective heat conductivities evaluated from the kinetic fluxes and fluid gradients were applied in the fluid code – and so on, until convergence. In a recent study [13], a Fokker-Planck kinetic model for electrons was coupled to a 1D fluid model in a similar way. However, these attempts are rather exotic and are not being used in the massive calculations with the 2D models.

VIII.1.3. Cross-field transport

Presently, there is no concise, credible theory that would describe anomalous plasma transport across the magnetic field (see Ch. VII for the present state of the theory in this area). In this situation, the most common approach is using the diffusive ansatz that meets at least the first law of thermodynamics. The "classical" cross-field diffusion of particles, parallel momentum and energy, which is related to the binary collisions between the charged particles that follow different orbits in the magnetic field, yields the values of the transport coefficients that are far too low to explain the radial profiles of the plasma parameters observed experimentally. There must be so-called "collective" effects related to some relatively small-scale turbulence, which are responsible for cross-field transport. These effects appear in the edge plasma models through the "anomalous" transport coefficients that are constructed to meet some empirical expectations, mostly, the radial profiles at the mid-plane of the plasma temperature and density or of the width of the power-carrying layer close to the separatrix in the SOL [15], [16]. Given the lack of detailed understanding of the processes causing the cross-field transport, the cross-field diffusivities are often set piecewise constant in the edge plasma. There have been attempts to adjust their profiles to reach a better match to the experimental measurements (see e.g. [17], [18], [19]). However, such an adjustment depends on the assumptions made for the parallel transport, the neutral transport, drifts and so on [20], [21] and is therefore not universal. The cross-field flow of particles naturally conveys the energy and parallel momentum.

Besides these diffusion-like flows, there are regular cross-field flows related to the macroscopic $\vec{E} \times \vec{B}$ drifts of the charged particles [22][23][24] and intermittent convection [25][26][27]. The drift-related flows are described rather strictly in the transport equations [15], but their inclusion in the computer models is still not routine. The complex picture of the magnetic drifts that cause electric currents that affect the distribution of the electric fields that

cause the $\vec{E}\times\vec{B}$ drift flows requires special effort to make the computations stable. We will discuss the drift effects in some more detail below.

The intermittent transport is less well understood. Experimentally, it is observed as a radial motion of some plasma structures ("blobs" or "filaments") aligned with the magnetic field [26]–[28]. There is some insight from theory into the nature of the radial transport of such coherent structures in the magnetic field [29], which predicts the velocity of their propagation, but no reliable model of formation of these "blobs" is available at present (see also Ch. VII). In the transport models, the intermittency is usually treated as time-average outward convection with a prescribed velocity [30], [31]. However, a simple model of the outward pinch has two principal drawbacks. First, the filaments (or "blobs") forming this flow contain the plasma with parameters close to those at the separatrix, which are very different from those of the background plasma in the far SOL, and this plasma does not mix with the background. On the contrary, the description of this flow by adding the convection velocity (or with the enhancement of the diffusivity) effectively mixes the blobs with the background. Whereas the fast-moving "blobs" can deliver a significant amount of the hot particles, before they spread along the field line and sink to the target, to the wall, thus forming some intermittent wall loading pattern, the slowly diffusing, average plasma has enough time to deposit it all onto the targets. This does also replace the heterogeneous plasma background for neutral transport with the homogeneous, averaged one. Given the non-linear, threshold nature of the dependence of the neutral penetration depth on the background plasma parameters, such averaging can introduce significant errors in the neutral penetration through the SOL [32]. Besides this, the blobs perturb the distribution of the electric potential in the edge plasma and can affect the $\vec{E}\times\vec{B}$-driven flows significantly [32]. The second drawback is that applying a prescribed outward velocity to all the species of the multi-component plasma, one over-estimates the impurity screening since the impurities are flushed away with the convection. Moreover, applying any prescribed convection velocity to the impurity ion transport can be physically wrong. Indeed, given the apparent interchange nature of the blobs, their propagation outwards must cause correspondingly enhanced inward transport of the background plasma. One can easily assume that the bulk, hydrogenic ions are more abundant closer to the separatrix, so their net "convective" flow is directed outwards. However, for the impurities, this is not always the case. Therefore, for physically correct modeling of intermittent, "blobby" transport in 2D transport models, one needs to take into account both the heterogeneity of the plasma parameters and the presence of the effective backflow of the background plasma.

A first step to producing a model of this kind was made in [33]. An approach of including the blob dynamics in a transport model by averaging over the ensemble of the blobs was developed there; however, the size and velocity of the blobs, as well as their starting location are still external parameters in the model. The blobs are 3D structures that occupy the full poloidal extent of the outboard SOL when mapped onto the (R, Z) plane. Combining multiple single blobs (which can be interpreted as time averaging) into a single "macro-blob" that travels across the SOL plasma without interaction allows one to solve the equations describing the propagation of the 3D filament in the framework of the 2D plasma solver (UEDGE in [33]). Such an approach provides a description of the intermittent wall loading and introduces to some extent a heterogeneous plasma background for interaction with neutrals, as well as the plasma backflow that is mimicked by the "bypass" that transfers the plasma from the blob front immediately to its wake. However, the effect of this approach on the electric fields – and hence on the $\vec{E}\times\vec{B}$ drifts – is not yet clear. Indeed, in this approach, a single macroscale circulation around the macro-blob replaces a set of fluctuating mesoscale circulations around every single blob. A similar concern

arises regarding the heterogeneity of the plasma background in this model. Here the macro-blob acts like a piston effectively screening the neutrals that recycle off the sidewalls, whereas the ensemble of the single, poloidally localized blobs leaves a gap for neutral penetration.

VIII.2. Neutral transport models

The neutral particles play an important role in the processes occurring in the edge plasma [34]. They are not affected by the magnetic field, so their transport is different from that of the charged components of the plasma. Eqs. (VIII.1) contain the source terms describing also the interactions between the charged and neutral particles and in order to calculate these terms, one needs a proper model for neutral transport. The distribution of the neutrals in the plasma edge depends, in particular, on the plasma parameters - hence the equations describing the neutrals must be solved together with Eqs. (VIII.1) and the corresponding blocks of the code realizing the model must be coupled. From the coupling viewpoint, the fluid equations for neutral transport similar to Eqs. (VIII.1) would be the most natural choice. However, this implies short mean-free-path of neutrals with respect to neutral-ion or neutral-neutral collisions, which, except for the regions of high plasma density, can be longer than the scale length of the profiles of the plasma parameters. Furthermore, because of the absence of interaction with the magnetic field, the neutral transport has no preferential direction and should be described in full 3D, which is computationally demanding. Therefore, kinetic, Monte-Carlo type modeling is mostly used in the major codes for edge plasma modeling for high fidelity simulations.

VIII.2.1. Fluid description of neutrals

Because of relative simplicity - compared with the kinetic model - the fluid-like models for neutral transport in the divertor received considerable attention from the developers of the edge modeling codes [35]–[40]. These models rely on the relaxation of the distribution function of hydrogen isotope atoms towards the ion distribution function in charge-exchange collisions with the plasma ions [35] since the neutral-neutral collisions are usually too seldom to establish the Maxwellian distribution of neutral species (see section IV.5 for more detail). The models are of different complexity; some of them take into account wall reflection and volumetric recombination and provide sources of particles, momentum and energy for Eq. (VIII.1). Their comparison with kinetic, Monte-Carlo models shows reasonable agreement, but for restricted Monte-Carlo models that describe the hydrogenic atoms only [41]. However, the importance of molecule transport in the description of divertor performance was clearly demonstrated using the full kinetic Monte-Carlo neutral model (see e.g. [42]) and the results obtained with a fluid neutral model differ, sometimes even qualitatively, from those obtained with the kinetic model [37]. Besides the lack of molecules in the fluid models, there are several other reasons for this difference. The radial profiles of the plasma parameters outside the separatrix are quite narrow, so the condition of smallness of the ratio of the neutral mean-free-path to the scale length of variation of the plasma parameters, necessary for validity of the fluid closure of the transport equations, is violated for neutrals in most of the edge plasma, except for the dense divertor regions close to the targets. It is difficult to describe correctly in a fluid model all the vast variety of physical processes that occur in collisions involving the neutral particles in the plasma and on the wall, as well as the geometry detail of the particular divertor configuration. In addition, the validity of the assumption of charge-exchange relaxation is not obvious for the impurity atoms.

There have been efforts to produce a hybrid, fluid-kinetic model for the neutral transport in the edge plasma [43]–[45], which would either apply kinetic corrections to the transport

coefficients or use either the fluid or the kinetic description in different regions of the calculation volume, but the applicability of such a model is still to be shown.

VIII.2.2. Monte-Carlo models

The mainstream approach to describing neutral particle transport in the edge plasma is presently direct Monte-Carlo modeling [46], [47]. In this, stochastic, approach, instead of solving the kinetic equations, Eq. (VI.1), directly, one models trajectories of the test particles, playing their interactions with the fixed background with the use of the pseudo-random numbers generated by the computer. The source terms for Eq. (VIII.1) are evaluated by calculating their intensity along the particle trajectory and summing it over the trajectories in each grid cell. This method is versatile with respect to the geometry of the problem, the composition of the particles considered and the choice of different reactions they participate in by collisions with the background particles. The latter represent, first of all, the electrons and ions of the plasma. In non-linear models, where the neutral-neutral interactions or radiation transport are included, the corresponding background is calculated in iterations on a grid of trilateral cells, which covers the regular grid used for solving Eqs. (VIII.1) plus the space between this grid and the material walls [42], [48]–[50]. The geometry can be arbitrarily complex, including sometimes 3D objects such as downpipes [51] or treating the full 3D configuration in a combination with a 3D plasma solver [52]. The selection of the test particles and background species, as well as of the reactions between them, is virtually unlimited – provided that the necessary cross-section or rate data are available. These data are normally imported from external databases [53] that are expandable. All this makes the Monte-Carlo approach very flexible and convenient.

However, the Monte-Carlo approach has three principal drawbacks. First, the numerical noise is always present in the solution because of a finite number of the test particles traced, and this noise reduces but slowly with an increase of this number. Therefore, Eqs. (VIII.1) become a set of differential equations with noisy sources, which creates certain problems for the numerics. In particular, the high-order discretization of Eqs. (VIII.1) [5] becomes inefficient when a Monte-Carlo package is used to compute the sources. Given the non-linear nature of Eq. (VIII.1), even a purely random noise on the source terms there can produce bias on the solution [54]. There are different sampling methods proposed [55], which reduce the noise by using some information from previous iterations, either correlating the pseudo-random number sequences between the iterations or by averaging the results over a certain number of iterations. These methods are still under development and are not routinely used in the 2D modeling applications, although some studies show their efficiency, see e.g. [56].

Secondly, the calculations become slow, especially when the geometry or reaction detail need to be resolved [57]. This problem can be alleviated by the use of parallel computing, but this still requires considerable computer resources. Apart from this, parallelization is efficient when one wants to suppress the noise by a significant increase of the number of the test particle histories followed. However, in the coupled fluid-kinetic calculations, the optimal strategy usually relies on keeping the noise at a certain level, so that it does not prevent reducing its effect by reducing the time step in the fluid code iterations. Pretty often it is the run time that determines the level of detail set up in the model: the runs may take months [57].

The third problem is related to the different treatment of the time dependence of the solution. Whereas Eqs.(VIII.1) describe the evolution of the edge plasma parameters, the standard Monte-Carlo approach assumes a steady state. It can be justified if the evolution of the plasma parameters is much slower than the relaxation of the neutral distribution, but this is not

always the case. This inconsistency is the source of difficulties by coupling the neutral and plasma models, which is discussed in the next section. A modification of the Monte-Carlo algorithm that includes time dependence in the particle tracing was proposed [58]. In some sense, it includes the time as one more dimension in modeling [47]. However, the practical realization of this approach [53], [58] leads to a significant increase of the numerical noise if the particle mean-free path in this "time" direction is longer than the time step in the iterations solving Eqs. (VIII.1).

VIII.2.3. Coupling to the plasma model

Coupling the neutral model based on differential equations to the plasma transport model has no principal problem. One simply adds to the system (VIII.1) some more equations of a similar structure, which requires no special measures to ensure compatibility between the two parts. However, when the Monte-Carlo approach is in effect, a problem arises. Whereas an implicit numerical scheme is normally used for advancing the discrete analog of Eqs. (VIII.1) in time, the Monte-Carlo description is explicit. This means that the neutral-related sources in Eqs. (VIII.1) are consistent with the plasma parameters before each time step, when the Monte-Carlo algorithm is applied, but the plasma parameters consistent with these sources are only available after the time step. Such discrepancy results in the appearance of parasitic sources in Eqs. (VIII.1) [57]. These sources, at a percent level, are not very important in the energy equations since the global energy balance in the edge plasma is sustained by equilibration of strong terms – the power input, volumetric losses and power delivered to the targets. They are probably not so important in the momentum equations also. However, in particle balance, these tiny sources may become comparable with the primary players, the fueling and pumping fluxes. Indeed, in the high recycling or detached divertor regime, see Ch. IX, the particle sources related to recombination of plasma ions and ionization of recycling neutrals can be much stronger than the fueling and pumping fluxes. Therefore, a percent level error in the recycling sources can act as an order of unity error in balance of pumping and fueling, which determines the density level or the particle content of the edge plasma, which, in turn, controls the divertor performance. A straightforward way from this problem would be reducing the time step in the iterations with Eqs. (VIII.1); however, this is time-consuming and often impractical.

A correction scheme proposed in [57], which yields the correction factors close to 1 for the ionization sources, which are found by solving the non-linear algebraic equations for global particle balance in the internal iterations foreseen anyway on each time step to cope with the non-linearity of the coefficients that appear in Eqs. (VIII.1), allows one to resolve the pumping and fueling fluxes in high recycling conditions within reasonable computational time, Fig. VIII.2. Note that neglect of these iterations for speeding up the computations may lead to a solution "converging" numerically well to very different profiles of the plasma parameters, which do not satisfy particle balance [59].

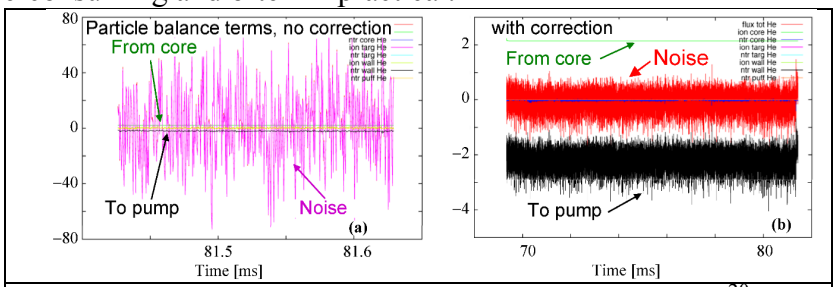

Fig. VIII.2. Time traces of different terms (fluxes in 10^{20}/s) in integral particle balance for helium, without (a) and with (b) the correction (note different vertical scale on the two plots). Reproduced with permission from [57], © Elsevier 2011.

VIII.3. Selection of constraints

The selection of the constraints for solving the transport equations is of primary importance when performing the modeling. Whereas the equations describe the interactions within the transport model, the constraints specify its interaction with the world external to the model, such as the plasma-wall interaction or external sources of energy, particles and momentum. In order to facilitate interpretation of the modeling results, the boundary conditions must be physically meaningful. Computationally, the most efficient constraints would be the first-type boundary conditions that specify the values of the quantities described by the transport equation – such as the temperature or density. However, the results obtained this way can be difficult to interpret. The fluxes on the boundary surfaces, which characterize interaction with the material of the plasma-facing elements or with the core plasma, can have very peculiar values that correspond e.g. to heating the plasma by the contact with the wall or to the particle outflow from the core well beyond the realistic values of the core fueling. This would require adjusting the boundary values and re-running the code until it converges to something reasonable.

VIII.3.1. Boundary conditions at the targets

At the targets, where the plasma flows onto the surface and is neutralized, the electrostatic sheath is formed (see Ch. IV), which corresponds to the electrical current closing through the surface (zero in the simplest case of the ambipolar flow). The boundary conditions discussed in Ch. IV are applicable here. Usually, one specifies the flow Mach number of 1 or greater than 1 and the sheath transmission factors $\gamma_{i,e}$ that relate the power and particle fluxes to the surface with the plasma temperature at the sheath entrance

$$q_{i,e} = \gamma_{i,e} j_{i,e} T_{i,e} , \qquad \text{(VIII.2)}$$

where $q_{i,e}$ are the energy fluxes carried by the ions and electrons and $j_{i,e}$ the corresponding particle fluxes. The sheath transmission factors are calculated using simplified distribution functions at the sheath entrance, see Ch. IV. Their typical values for the case of Eq. (VIII.1) written for the full energy, absence of the secondary electron emission and the plasma flow Mach number of unity at the sheath are $\gamma_i \sim 3$ and $\gamma_e \sim 5$ (note that these values should be taken with caution). Although Eq. (VIII.2) appears to specify the power flux depending on $\gamma_{i,e}$, it is used to find the temperature since the fluxes are determined by the sources.

VIII.3.2. Boundary conditions at the core boundary

This boundary describes the interaction with the core plasma. The primary role of the core in the edge modeling is supplying the power since there is no other source of energy in the edge. The most natural choice for the boundary conditions there is specifying the power flux across this boundary in the ion and electron channels. The total power flux is determined by the heating of the core plasma from the external sources (the plasma current, neutral beams, electron cyclotron waves, etc.) or from the fusion reactions, and the radiation power losses from the core. In principle, its distribution over the core boundary is non-uniform – one can expect higher fluxes on the outboard side due to ballooning effects. In practice, this flux is usually specified uniform and the ballooning effects are simulated to a certain extent by non-uniform radial transport between this boundary and the separatrix, either because of the Shafranov's shift of the magnetic flux surfaces outwards due to a finite plasma pressure, or by prescribing the spatially non-uniform diffusivities.

The core plasma can also be a source of the plasma particles that originate either from the external sources (beams, pellets) or from the neutrals penetrating the core boundary from the edge, or from the time evolution of the core plasma density. (In the latter case, the core boundary source of particles can become negative if the core density grows, reflecting core fueling by the plasma influx from the edge). Here also, specification of the particle fluxes across the core boundary is the best choice from the physics viewpoint, since these fluxes are usually well determined by the particle sources in the core. For the parallel momentum transport equation, either the zero parallel velocity (no core rotation) or zero flux of the parallel momentum across the core boundary (core rotation not related to the edge) is usually applied if no drifts are taken into account. This should create no problem since in most cases, the parallel velocity of all plasma components near the core boundary is low – the flows are well subsonic. However, plasma rotation can affect the electric fields forming there, so one may need to think some more if working with the drifts and currents [15].

VIII.3.3. Boundary conditions at the "radial" edges of the grid

The boundary conditions at the grid edges facing the first wall or the PFR (lines BCD and AFE in Fig. VIII.1) have not received much attention when the grid does not reach the wall. There is not so much power reaching there, so the conditions at these boundaries should have no strong impact on the first target of the modeling: the power loading of the divertor targets. Usually, one sets a third type boundary condition here, which relates the radial energy or particle flux at the boundary to the particle or energy density there via prescribing the convective flux with specified velocity. Sometimes this is done through specifying the "decay length" of the temperature and density profiles [57], sometimes by specifying the effective convective velocities directly [15]. For the parallel momentum, either the slippage (zero radial flux) or sticking (zero flow velocity) condition is usually applied at this boundary.

VIII.3.4. Fueling constraints

The way of specifying the level of plasma density in the computational model requires special attention. The most natural parameter to use for this purpose would be the total, ion plus neutral, particle content outside the separatrix [60], [61]. This quantity, N_{tot}, can be described by the particle balance equation that is only weakly related to the edge plasma solution and so can be considered a truly external, controllable parameter. Typically, N_{tot} changes slowly and smoothly by variation of the fueling rate and it is the parameter directly affected by gas puffing and pumping in the experiment. However, in the experiment, N_{tot} is practically not measurable. Therefore, one needs to find a constraint that would represent N_{tot} and be physically meaningful and measurable, in order to allow comparisons with the experiment. In practice, the electron density at some point at the separatrix n_{sep} is often chosen as such a constraint [19][62][63]. Since n_{sep} cannot be used directly as the boundary condition (the separatrix lies inside the computational area), the constraint $n_{sep} = n_{sep}^{*}$ where n_{sep}^{*} is the required value of n_{sep}, is met by adjusting some other parameters, such as the particle flux from the core, the gas puffing rate or the cross-field transport coefficients. If the latter are fixed, the density control in the code run looks similar to that in the experiment. However, having n_{sep} as the target in the control system can result in artificial "bifurcations" in the code or sudden jump of the detachment front to the x-

point by increasing n_{sep}. Indeed, n_{sep} can be non-monotonic by the density ramp towards detachment [10]. It increases first with N_{tot}, then saturates and rolls over, and finally increases again, Fig. VIII.3. If the density is raised by controlling N_{tot}, the detachment evolves smoothly – a small variation of N_{tot} causes a small variation of the other parameters. However, if one controls the fueling rate trying to realize a smooth raise of n_{sep}, a "bifurcation" appears once n_{sep} reaches the rollover. At this point, a further increase of n_{sep} is only possible by a significant increase of N_{tot} and in terms of n_{sep}, a small variation of its value causes a significant change of the solution. This happens in modeling [62] and probably in the experiment when the upstream density is feedback-controlled.

Therefore, using N_{tot} as the density control parameter is preferable for the clearer physical interpretation of the modeling results [61]. However, this quantity is not very useful for analysis of the effects of coupling the edge to the core models. Using the neutral pressure p_n in front of the pumping duct entrance in the divertor may help in this case [64]. On the one hand, its relation to N_{tot} is usually monotonic. On the other one, it is related directly to the pumping throughput, which is one of the major parameters controlling the performance of the whole machine.

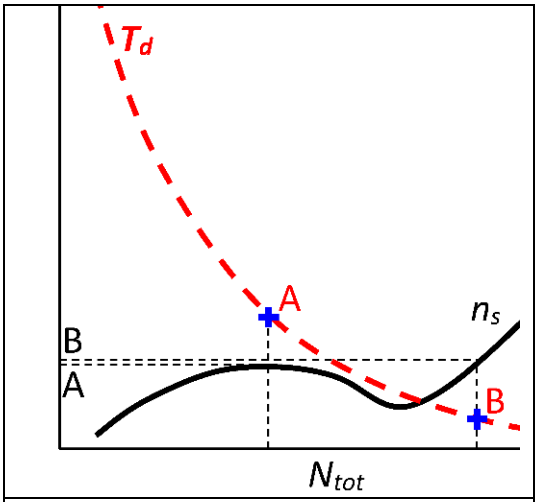

Fig. VIII.3. Schematics of "bifurcation" seen when the edge plasma density is characterized by the separatrix density n_{sep}. A small change in n_{sep} from level A to B corresponds to a significant increase of N_{tot}, which leads to a considerable change of the detachment state (represented here by the divertor plasma temperature T_d).

VIII.4. Physics results and model validation

Historically, modeling and experiment with a poloidal divertor have gone in parallel all the time, with modeling closely following the experiment and helping to interpret the experimental data. A comparison of the modeling results with experimental data serves as code validation and different groups pursue this activity permanently, following the improvements in the experimental diagnostics and development of the model. However, given the obvious lack of comprehensive physical description of the edge plasma, see Ch. VI and VII, this comparison can be rather tricky. In this chapter, we give examples of the application of modeling tools to several problems of the plasma edge physics, aiming at the qualitative understanding of relative importance of different processes involved and at confronting the experiments to validate the models. This is not a comprehensive review and we apologize for having not touched upon many other applications – in particular, the kinetics or turbulence codes.

VIII.4.1. 2D transport modeling

Looking broadly, one can see a good qualitative agreement between the general trends in the edge plasma in experiment and modeling, even without fine-tuning of the models. Such features are, for example, evolution of the power loading and particle flux onto the divertor target along

with an increase of the edge density (fueling) or impurity level (seeding) [65], appearance of plasma detachment at sufficient density or radiation level [66]–[68], or reduction of the upstream plasma density at the separatrix by impurity seeding [69], [19]. In particular, the effect of the $\vec{E}\times\vec{B}$ and ∇B drifts on the detachment asymmetry in H-mode was confirmed by comparing the UEDGE code results with DIII-D data from Thomson scattering diagnostics by different directions of the toroidal magnetic field [62]. However, a successful quantitative comparison of a modeling run with a single experimental shot, which is usually termed "model validation", is not easy. As was noted in [70], the codes can reproduce the experimental data satisfactorily for Ohmic and L-mode discharges with no significant plasma detachment from the targets. Since then, a considerable effort has been made to model experiments with H-mode plasma and detachment (see e.g. [71] [72] [19], [21] [62] [73]).

The most severe challenges in modeling the experiment are the in-out asymmetry of detachment and the appearance of the high-density region at the top of the inner divertor target in the far SOL. An example of modeling-to-experiment comparison is shown in Fig. VIII.4, where the density and temperature profiles in two DIII-D H-mode shots with different orientation of the toroidal magnetic field, obtained experimentally and modeled with UEDGE, are shown. All four cases feature the same electron density at the separatrix in the outer mid-plane. For the experimental profiles, the data from the Thomson scattering diagnostics covering well the divertor region were used. In the calculations, the $\vec{E}\times\vec{B}$ and ∇B drifts were switched on, which yielded a pronounced effect on the in-out asymmetry of density, qualitatively similar to the experimental observations. However, the high density in the far SOL near the inner target by the forward field is not reproduced and high density in the outer divertor appears by the reverse field in modeling but is not seen in the experiment. In this study aimed at qualitative demonstration of the drift effects, there was no attempt of tuning the model parameters to fit the experiment better. In particular, the cross-field diffusivities for particles and energy were taken spatially uniform and the impurity radiation was emulated by assuming a fixed relative concentration of C in the plasma.

For getting closer to the experiment, the usual practice is to adjust the radial profiles of the cross-field transport coefficients to fit the upstream profiles of n and T. This procedure allows one to reach a reasonable agreement between the experimental measurements and the plasma profiles at the mid-plane, Fig. VIII.5, and in divertors, Fig. VIII.6, but it often involves strong enhancement of the diffusivities in the far SOL [75], [21], [76] and sometimes the introduction

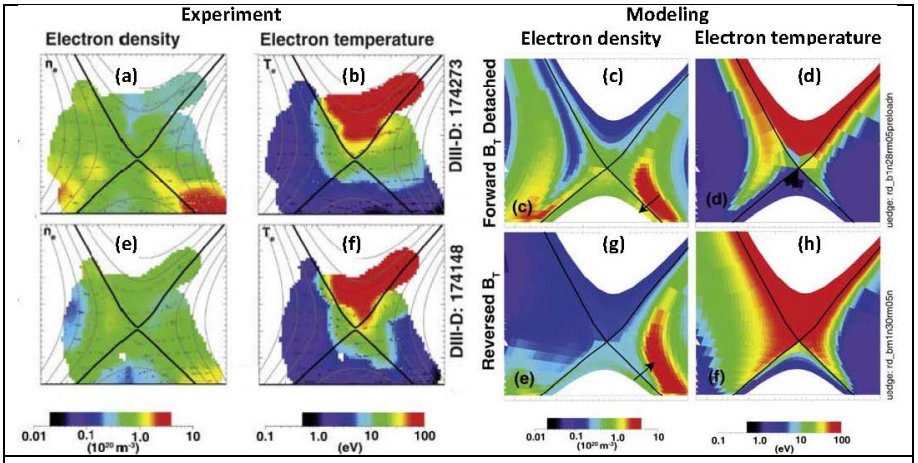

Fig. VIII.4. Density (a, c, e, g) and temperature (b, d, f, h) profiles in the DIII-D divertor, measured from Thomson scattering (a, b, e, f) and calculated with UEDGE for the "forward" ($\vec{B}\times\nabla B$ drift directed downwards) (c, d) and "reverse" (g, h) orientation of the toroidal magnetic field. The gray dots on the experimental figures indicate the locations of the measurements. Reproduced with permission from [74], © Elsevier 2019.

of outward particle convection [30][21]. Then, in the absence of the drifts in the model, one has to introduce a strong poloidal variation of the cross-field diffusivities, which now increase significantly in the divertor region [77]. This allows one to reproduce the roll-over of the ion saturation current, I_{sat}, measured by probes in JET, at a lower upstream plasma density, closer to the experimental values, and the in-out asymmetry of the temperature and pressure drop towards the targets by detachment. However, the roll-over of the I_{sat} in the inner and outer divertors occurs at nearly the same value of the upstream density – that is, both divertors start to detach simultaneously, whereas in the experiment, the inner one detaches first. This model does also not reproduce the high density in the far SOL at the inner target (Fig. VIII.4a), seen on different machines. Only simultaneous activation of all the drifts and currents, variable cross-field transport and detailed simulation of impurity transport in the multi-fluid code [21] allowed one to see this effect in modeling.

However, this, at least, qualitative agreement with the experiment requires specification of rather peculiar profiles of the radial transport coefficients. An example of these profiles used for reproducing the measurements on ASDEX Upgrade and JET [76] is shown in Fig. VIII.5. These coefficients vary also in the poloidal direction to reflect the ballooning nature of the radial transport. Profiles of this kind are typical in the "model validation" studies (see also [75], [78], [15], [21]). Looking at the diffusivities required in the far SOL, one finds that they are often significantly higher than the Bohm diffusivity. For example, the value of ~30 m^2/s for χ_e (Fig. VIII.5) corresponds to the Bohm diffusivity at ~ 900 eV – the value that can hardly be expected in the far SOL. Since the Bohm expression is seen as the upper limit of the diffusivity driven by electrostatic turbulence, see Ch. VII, one can conclude that radial plasma transport in the far SOL is dominated by some

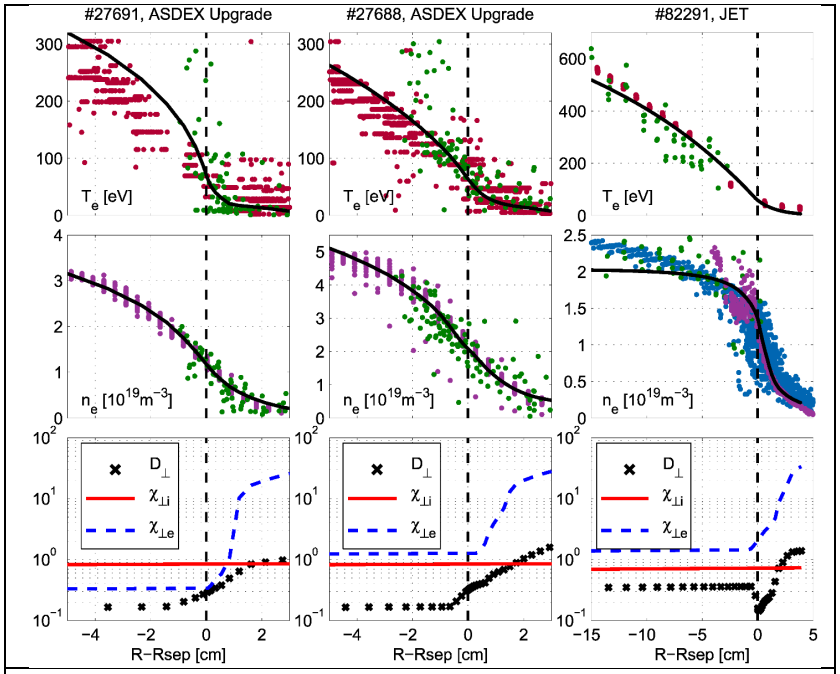

Fig. VIII.5. The measured and modeled profiles of T_e (top row), n_e (middle row), and the specified transport coefficients ($D_\perp$, χ_i, χ_e, bottom row, (m^2 s^{-1})) at the outer midplane. The temperature measurements are obtained from the Electron Cyclotron Emission (red) and Thomson scattering (green), and the density measurements are from the Integrated Data Analysis (purple, AUG), Li-beam (purple, JET), reflectometry (blue, JET) and Thomson scattering (green). The IDA profile in ASDEX Upgrade is obtained as a combination of the Li-beam and the laser diagnostics. Based on the uncertainties in the radial positioning of the diagnostic data and the separatrix location, as well as the uncertainty range of the measurements, n_{sep} can vary between 0.8–1.6 × $10^{19}m^{-3}$ (#27691) and 1.5–2.8 × $10^{19}m^{-3}$ (#27688) in ASDEX Upgrade, and between 0.7–1.7 × $10^{19}m^{-3}$ in JET. Reproduced with permission from [76], © IOP Publishing 2017.

processes related to perturbation of the magnetic field or by outward convective transport there [29]. Since this convective flow is formed by filaments (hot plasma formations aligned with the magnetic field and traveling radially through the SOL), it is intermittent [75][26][28][27] and its inclusion into the 2D transport codes is not straightforward, see section VIII.1.3. It is sometimes emulated as an outward pinch – a convective velocity imposed on the top of diffusion transport in the equations (VIII.1) [30][21].

In the last decade, a considerable effort has been made to model the radial electric field E_r in the plasma edge using 2D transport codes (mostly, the SOLPS family) with drifts and currents. In the code, E_r is calculated from the electrostatic potential, whose distribution is found from Eq. (VI.52). In particular, the significant difference in the E_r values between the L and H modes is reproduced well by the code, thus indicating the neoclassical (drift-related) nature of this field in the H-mode, Fig. VIII.7.

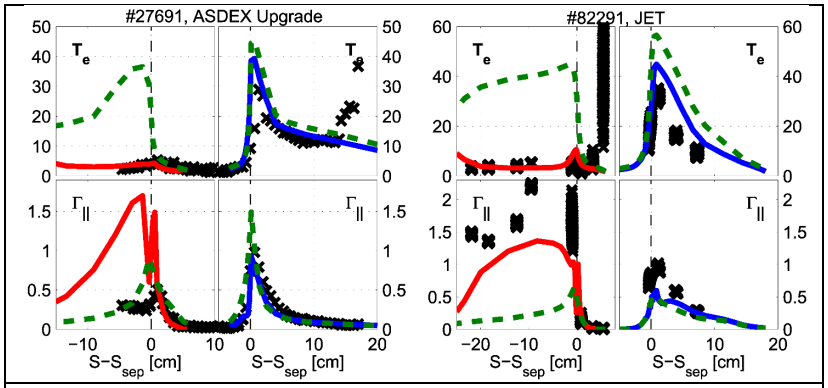

Fig. VIII.6. Comparisons between the modeled and measured target electron temperatures, T_e (eV), and ion fluxes, $\Gamma_{||}$ (10^{24} $m^{-2}s^{-1}$), top and bottom row, respectively. The results are shown for the ASDEX Upgrade discharge #27691 and for the JET discharge #82291 (the so-called low-density reference discharges). For both discharges, the inner divertor comparisons are shown on the left-hand side, and the outer divertor comparisons are on the right-hand side. The Langmuir probe measurements are drawn with black crosses, the simulations with drifts with solid lines (red and blue for the inner and outer divertor, respectively), and the simulations without drifts (but with the currents activated) with dashed green lines. Reproduced with permission from [76], © IOP Publishing 2017.

VIII.4.2. Modeling the 3D effects

The 2D models considered above assume the toroidal symmetry of the problem. In a real tokamak experiment, this symmetry is not maintained. The vacuum chamber has discreet ports (NBI, pumping, diagnostics, etc.) and protruding structures, such as limiters or ICRF antennas. The particle source from the gas puff or NBI is toroidally asymmetric. The external magnetic fields applied to the plasma are asymmetric and the plasma itself develops perturbations that are not toroidally symmetric (e.g., ELMs). Therefore, the results of the 2D modeling can only be considered as toroidally average and 3D models are needed to study these 3D effects in more detail.

The most published 3D transport codes for the edge plasma modeling are presently EMC3-Eirene [2] and JOREK [79]. EMC3-Eirene is a 3D Monte-Carlo code based on the stationary Braginskii equations for the plasma ions and electrons, coupled to the Monte-Carlo code Eirene that calculates the neutral-related sources in the plasma equations. It is a transport code that runs on a prescribed background magnetic field of nearly arbitrary complexity. JOREK is a finite-element, non-ideal MHD code that solves time-dependent, non-linear MHD and transport equations and calculates the perturbations of the magnetic field self-consistently. Naturally, the increase of the geometrical complexity requires some simplification of the transport models used

in these codes. Given the limited amount of the computational resources available, this is unavoidable.

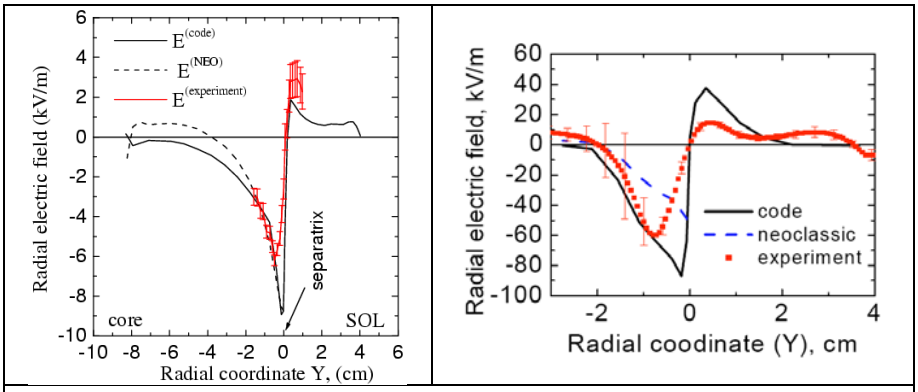

Fig. VIII.7. Radial electric field in the AUG Ohmic (left) and H-mode (right) shots, calculated with B2SOLPS5.0 code and measured by Doppler reflectometry, compared with the neoclassical values. Reproduced with permission from [80], © Elsevier 2011.

The EMC3-Eirene code was originally developed aiming at stellarator applications [52]. The growing interest to its application to tokamak modeling in last decades is related to the perspective of using the resonance magnetic perturbation (RMP) techniques to reduce the size of the ELMs that are seen as one of the key issues for the divertor lifetime in a fusion reactor-tokamak such as ITER [81]. The idea of this method is in introducing toroidally asymmetric, external coils carrying currents in order to disturb the magnetic surfaces at the plasma edge. A number of experiments performed on DIII-D [82], ASDEX Upgrade [83], JET [84], NSTX [85], MAST [86] tokamaks have shown that this scheme allows working in H-mode without Type I ELMs.

Effective stochastization of the flux surfaces around the separatrix results in a complex flow pattern that is qualitatively reproduced with EMC3-Eirene, Fig. VIII.8. The calculations reproduce also the increase of stochastization by the increase of the current in the RMP coils. However, the simplified transport model together with the prescribed magnetic field in the model (the currents appearing in such a 3D plasma effectively screen the perturbations [87][88], so the magnetic field depends on the plasma profiles and should be re-calculated consistently) do not allow good quantitative comparison.

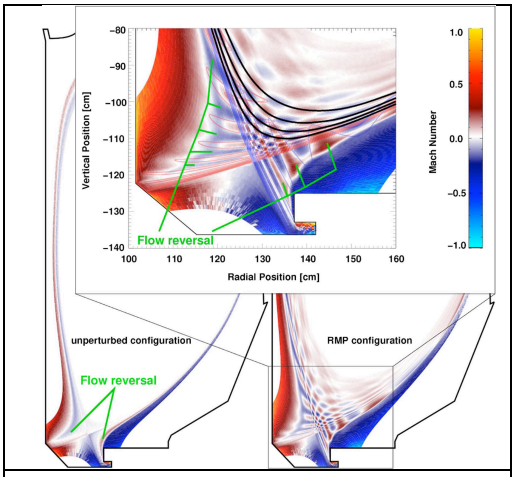

Fig. VIII.8. Parallel flow pattern in the edge plasma in unperturbed and perturbed magnetic configurations in DIII-D as calculated by EMC3-Eirene. The positive flow is directed from the outer target to the inner one. Reproduced with permission from [2], © IOP Publishing 2017.

However, for the problems that do not involve perturbation of the magnetic configuration, the situation is better. For example, a good quantitative comparison of EMC3-Eirene calculations and experimental data can be found in [89]. Here spreading of the plasma along the flux tubes by a toroidally and poloidally localized gas puff was modeled. This problem involves no self-adjusting of the magnetic field, so comparing the code results with the experiment is easier. The D_2 gas was injected locally at the inner mid-plane and the C^{2+} ion flow velocities were measured from the

Doppler shift of the emission lines around the gas injection location. The flow pattern was found to form a 3D structure aligned with the magnetic flux tubes, indicating an acceleration of C^{2+} ions by friction with the D^{+} ions spreading along the flux tubes from the gas injection position. The EMC3-Eirene calculations including the carbon impurity in the test fluid approximation reproduce the measured flow velocities reasonably well, Fig. VIII.9.

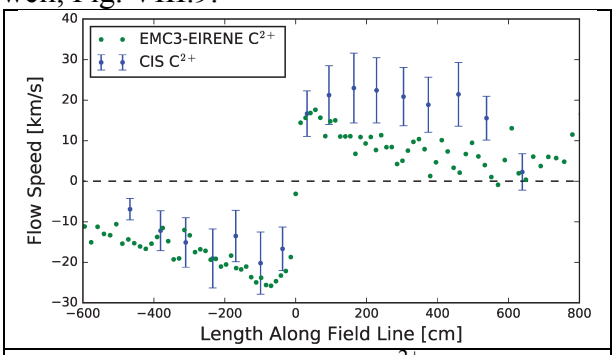

Fig. VIII.9. The measured C^{2+} ion velocity along a field line shown in blue. Green points are the C^{2+} parallel ion velocities as extracted from EMC3-EIRENE simulations. Reproduced with permission from [89], © IAEA 2018.

A phenomenon in the edge plasma, which is extremely challenging for modeling studies, is the appearance of ELMs. They appear as intense bursts of the energy and particle losses from the core plasma into the SOL in the H-mode [90]. The large (Type I) ELMs carry the energy sufficient to damage the target surfaces in a high-power experiment such as ITER [91]. The experimental data suggest that these bursts have a short duration and a pronounced 3D spatial structure. Several attempts of modeling ELMs in the framework of 2D transport models [92] [93] [94] by increasing strongly the cross-field transport coefficients for a short time and following propagation of the heat pulse produced on the non-disturbed magnetic field have mostly phenomenological value. The macro-blob approach described in section VIII.1 offers a more accurate description of the radial propagation of a large perturbation of the plasma parameters in the SOL by ELMs [95]. However, 3D perturbations of the magnetic field by ELMs remain outside the scope, so the ELM structure and the pattern of the power deposition on the targets and walls are not resolved.

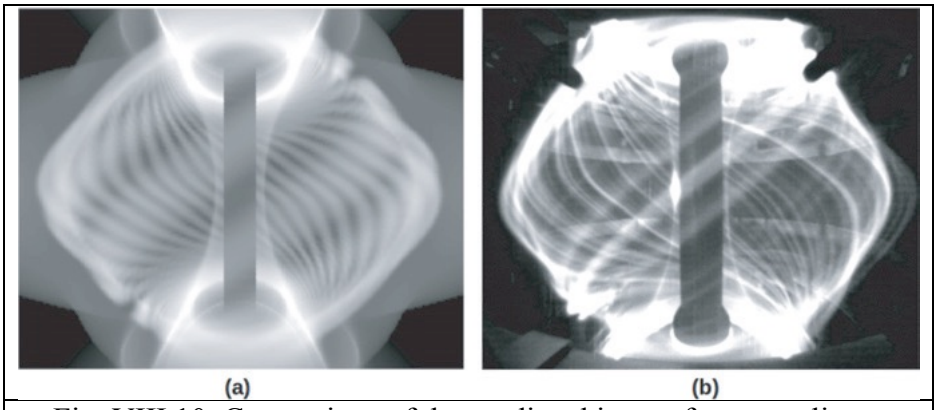

Fig. VIII.10. Comparison of the predicted image from non-linear MHD ELM simulation (a) with the visible camera image of an ELM in MAST (b). Reproduced with permission from [98], © IOP Publishing 2013.

Physically sound modeling of ELMs requires codes that combine 3D MHD and transport models, such as JOREK [96]. This code describes the dynamics of perturbations of the plasma parameters and magnetic field and is capable of following the non-linear stage of development of non-ideal MHD instabilities. The code reproduces well the structure of the plasma perturbations by the ELM crash, Fig. VIII.10. More quantitative comparisons involve experiments on ASDEX Upgrade [97], JET [96], MAST [98] and others. They include analysis of the structure of the unstable modes and their interactions that lead to the ELM crash, of mechanisms of the energy and particle loss from the core plasma by ELMs, and of different ways to the ELM control and mitigation.

Conclusions for Ch. VIII

Summarizing this chapter, we can say that although the models can reproduce many of the experimental features of the divertor plasmas, their correct application is not a routine procedure and it requires serious consideration for each particular situation in each particular device. None of the models used is complete, even within the restricted range of the time scales of the processes modeled. Given the remaining uncertainty in the description of the plasma transport, one needs to perform a large number of the code runs in order to reveal inter-dependencies between the plasma parameters and to project them onto the experiment. This brings the computational efficiency of the models to the same level of importance as the physical accuracy, so the trade-off between the code efficiency and the completeness of the physical model is the principal issue that determines the success of a modeling study [57].

References for Chapter VIII

[1] A. S. Kukushkin and S. I. Krasheninnikov, "Bifurcations and oscillations in divertor plasma," *Plasma Phys. Control. Fusion*, vol. 61, no. 7, p. 74001 (8pp), 2019.

[2] Y. Feng, H. Frerichs, M. Kobayashi, and D. Reiter, "Monte-Carlo fluid approaches to detached plasmas in non-axisymmetric divertor configurations," *Plasma Phys. Control. Fusion*, vol. 59, no. 3, p. 034006 (16pp), 2017.

[3] R. Simonini, G. Corrigan, G. Radford, J. Spence, and A. Taroni, "Models and Numerics in the Multi-Fluid 2-D Edge Plasma Code EDGE2D/U," *Contrib. to Plasma Phys.*, vol. 34, no. 2–3, pp. 368–373, 1994.

[4] D. P. Coster *et al.*, "Further Developments of the Edge Transport Simulation Package, {SOLPS}," in *Proc. of the 19th IAEA Conference, Fusion Energy, Lyon, France, October 2002, (CD-ROM)*, 2002, p. IAEA-CN-94/TH/P2-13.

[5] T. D. Rognlien, J. L. Milovich, M. E. Rensink, and G. D. Porter, "A fully implicit, time dependent 2-D fluid code for modeling tokamak edge plasmas," *J. Nucl. Mater.*, vol. 196–198, pp. 347–351, 1992.

[6] T. Eich *et al.*, "Scaling of the tokamak near the scrape-off layer H-mode power width and implications for ITER," *Nucl. Fusion*, vol. 53, no. 9, p. 093031 (7pp), 2013.

[7] H. J. Sun *et al.*, "Study of near SOL decay lengths in ASDEX Upgrade under attached and detached divertor conditions," *Plasma Phys. Control. Fusion*, vol. 59, no. 10, p. 105010 (11pp), 2017.

[8] H. Bufferand *et al.*, "Numerical modelling for divertor design of the WEST device with a focus on plasma-wall interactions," *Nucl. Fusion*, vol. 55, no. 5, p. 053025 (9pp), 2015.

[9] W. Dekeyser, M. Baelmans, D. Reiter, P. Börner, and V. Kotov, "2D edge plasma modeling extended up to the main chamber," *J. Nucl. Mater.*, vol. 415, no. 1 SUPPL, pp. S584–S588, Aug. 2011.

[10] S. I. Krasheninnikov and A. S. Kukushkin, "Physics of ultimate detachment of a tokamak divertor plasma," *J. Plasma Phys.*, vol. 83, no. 05, p. 155830501 (77pp), 2017.

[11] S. I. Braginskii, "Transport processes in a plasma," in *Reviews of Plasma Physics vol. 1*, New York: Consultants Bureau, 1965, p. 205.

[12] A. S. Kukushkin and A. M. Runov, "Implementation of non-local transport model into 2D fluid code," *Contrib. to Plasma Phys.*, vol. 34, no. 2/3, pp. 204–209, 1994.

[13] M. Zhao and A. Chankin, "SOLPS simulations with electron kinetic effects," *Plasma Phys. Control. Fusion*, vol. 61, no. 2, p. 025019 (11pp), 2019.

[14] P. L. Bhatnagar, E. P. Gross, and M. Krook, "A Model for Collision Processes in Gases. I. Small Amplitude Processes in Charged and Neutral One-Component Systems," *Phys. Rev.*, vol. 94, no. 3, pp. 511–525, 1954.

[15] V. Rozhansky *et al.*, "New B2SOLPS5.2 transport code for H-mode regimes in tokamaks," *Nucl. Fusion*, vol. 49, no. 2, p. 025007 (11pp), 2009.

[16] A. S. Kukushkin, H. D. Pacher, G. W. Pacher, V. Kotov, R. A. Pitts, and D. Reiter, "Consequences of a reduction of the upstream power SOL width in ITER," *J. Nucl. Mater.*, vol. 438, no. SUPPL, pp. S203–S207, 2013.

[17] W. Fundamenski, S. Sipilä, and JET-EFDA Contributors, "Boundary plasma energy transport in JET ELMy H-modes," *Nucl. Fusion*, vol. 44, no. 1, pp. 20–32, 2004.

[18] S. Wiesen *et al.*, "Effect of PFC Recycling Conditions on JET Pedestal Density," *Contrib. to Plasma Phys.*, vol. 56, no. 6–8, pp. 754–759, 2016.

[19] F. Reimold *et al.*, "Experimental studies and modeling of complete H-mode divertor

detachment in ASDEX Upgrade," *J. Nucl. Mater.*, vol. 463, pp. 128–134, 2015.
[20] A. S. Kukushkin and H. D. Pacher, "Critical evaluation of the determination of the SOL transport mechanism from a statistical examination of experimental data," *Contrib. to Plasma Phys.*, vol. 46, no. 7–9, pp. 545–550, 2006.
[21] F. Reimold *et al.*, "The high field side high density region in SOLPS-modeling of nitrogen-seeded H-modes in ASDEX Upgrade," *Nucl. Mater. Energy*, vol. 12, pp. 193–199, 2017.
[22] M. Baelmans, D. Reiter, and R. R. Weynants, "New Developments in Plasma Edge Modeling with Particular Emphasis on Drift Flows and Electric Fields," *Contrib. to Plasma Phys.*, vol. 36, no. 2–3, pp. 117–126, 1996.
[23] T. D. Rognlien, D. D. Ryutov, N. Mattor, and G. D. Porter, "Two-dimensional electric fields and drifts near the magnetic separatrix in divertor tokamaks," *Phys. Plasmas*, vol. 6, no. 5, pp. 1851–1857, 1999.
[24] A. V. Chankin and P. C. Stangeby, "Contribution of the ion diamagnetic flow to poloidal rotation and pressure asymmetries in the SOL," *Nucl. Fusion*, vol. 41, no. 4, pp. 421–429, 2001.
[25] J. R. Myra *et al.*, "Blob birth and transport in the tokamak edge plasma: Analysis of imaging data," *Phys. Plasmas*, vol. 13, no. 9, p. 092509 (10pp), 2006.
[26] J. A. Boedo *et al.*, "Transport by intermittent convection in the boundary of the DIII-D tokamak," *Phys. Plasmas*, vol. 8, no. 11, pp. 4826–4833, 2001.
[27] A. Kirk *et al.*, "Filament structures at the plasma edge on MAST," *Plasma Phys. Control. Fusion*, vol. 48, no. 12 B, pp. B433–B441, 2006.
[28] J. A. Boedo *et al.*, "Transport by intermittency in the boundary of the DIII-D tokamak," *Phys. Plasmas*, vol. 10, no. 5 II, pp. 1670–1677, 2003.
[29] S. I. Krasheninnikov, "On scrape off layer plasma transport," *Phys. Lett. Sect. A Gen. At. Solid State Phys.*, vol. 283, no. 5–6, pp. 368–370, 2001.
[30] A. Y. Pigarov, S. I. Krasheninnikov, T. D. Rognlien, M. J. Schaffer, and W. P. West, "Tokamak edge plasma simulation including anomalous cross-field convective transport," *Phys. Plasmas*, vol. 9, no. 4, pp. 1287–1299, 2002.
[31] A. Y. Pigarov, S. I. Krasheninnikov, B. LaBombard, and T. D. Rognlien, "Simulation of large parallel plasma flows in the tokamak SOL driven by cross-field transport asymmetries," *J. Nucl. Mater.*, vol. 363–365, pp. 643–648, 2007.
[32] S. I. Krasheninnikov, A. Y. Pigarov, T. K. Soboleva, and D. L. Rudakov, "Strongly intermittent edge plasma transport: Issues with modeling and interpretation of experimental data," *Phys. Plasmas*, vol. 16, no. 1, p. 014501 (4pp), 2009.
[33] A. Y. Pigarov, S. I. Krasheninnikov, and T. D. Rognlien, "New approach in two-dimensional fluid modeling of edge plasma transport with high intermittency due to blobs and edge localized modes," *Phys. Plasmas*, vol. 18, no. 9, p. 092503 (12 pp), 2011.
[34] A. S. Kukushkin and H. D. Pacher, "Neutral recirculation - The key to control of divertor operation," *Nucl. Fusion*, vol. 56, no. 12, p. 126012 (7pp), 2016.
[35] P. Helander, S. I. Krasheninnikov, and P. J. Catto, "Fluid equations for a partially ionized plasma," *Phys. Plasmas*, vol. 1, no. 10, pp. 3174–3180, 1994.
[36] D. Knoll, P. R. McHugh, S. I. Krasheninnikov, and D. J. Sigmar, "Simulation of dense recombining divertor plasmas with a Navier–Stokes neutral transport model," *Phys. Plasmas*, vol. 3, no. 1, pp. 293–303, 1996.
[37] M. Furubayashi *et al.*, "Comparison of kinetic and fluid neutral models for attached and

detached state," *J. Nucl. Mater.*, vol. 390–391, no. 1, pp. 295–298, 2009.
[38] M. E. Rensink, L. Lodestro, G. D. Porter, T. D. Rognlien, and D. P. Coster, "A Comparison of Neutral Gas Models for Divertor Plasmas," *Contrib. to Plasma Phys.*, vol. 38, no. 1-2, pp. 325–330, 1998.
[39] J. Riemann, M. Borchardt, R. Schneider, A. Mutzke, T. Rognlien, and M. Umansky, "Navier-stokes neutral and plasma fluid modelling in 3d," *Contrib. to Plasma Phys.*, vol. 44, no. 1-3–3, pp. 35–38, 2004.
[40] K. Hoshino *et al.*, "Benchmarking kinetic and fluid neutral models with drift effects," *Contrib. to Plasma Phys.*, vol. 48, no. 1–3, pp. 136–140, 2008.
[41] N. Horsten, W. Dekeyser, G. Samaey, and M. Baelmans, "Assessment of fluid neutral models for a detached ITER case," *Nucl. Mater. Energy*, vol. 12, pp. 869–875, 2017.
[42] A. S. Kukushkin, H. D. Pacher, V. Kotov, D. Reiter, D. Coster, and G. W. Pacher, "Effect of neutral transport on ITER divertor performance," *Nucl. Fusion*, vol. 45, no. 7, pp. 608–616, 2005.
[43] C. F. Karney, D. P. Stotler, and B. J. Braams, "Modeling of neutral plasma in a divertor in the fluid-kinetic transition," *Contrib. Plasma Phys.*, vol. 38, no. 1–2, pp. 319–324, 1998.
[44] N. Horsten, G. Samaey, and M. Baelmans, "Hybrid fluid-kinetic model for neutral particles in the plasma edge," *Nucl. Mater. Energy*, vol. 18, pp. 201–207, 2019.
[45] M. Blommaert, N. Horsten, P. Borner, and W. Dekeyser, "A spatially hybrid fluid-kinetic neutral model for SOLPS-ITER plasma edge simulations," *Nucl. Mater. Energy*, vol. 19, pp. 28–33, 2019.
[46] D. Stotler and C. Karney, "Neutral Gas Transport Modeling with DEGAS 2," *Contrib. to Plasma Phys.*, vol. 34, no. 2–3, pp. 392–397, 1994.
[47] D. Reiter, M. Baelmans, and P. Börner, "The EIRENE and B2-EIRENE Codes," *Fusion Sci. Technol.*, vol. 47, no. 2, pp. 172–186, 2005.
[48] D. Reiter, S. Wiesen, and M. Born, "Towards radiation transport modelling in divertors with the EIRENE code," *Plasma Phys. Control. Fusion*, vol. 44, no. 8, pp. 1723–1737, 2002.
[49] V. Kotov, D. Reiter, A. S. Kukushkin, H. D. Pacher, P. Börner, and S. Wiesen, "Radiation absorption effects in B2-EIRENE divertor modelling," *Contrib. to Plasma Phys.*, vol. 46, no. 7–9, pp. 635–642, 2006.
[50] D. Reiter, V. Kotov, P. Börner, K. Sawada, R. K. Janev, and B. Küppers, "Detailed atomic, molecular and radiation kinetics in current 2D and 3D edge plasma fluid codes," *J. Nucl. Mater.*, vol. 363–365, no. 1–3, pp. 649–657, 2007.
[51] S. Lisgo *et al.*, "OSM-EIRENE modeling of neutral pressures in the Alcator C-Mod divertor," *J. Nucl. Mater.*, vol. 337–339, pp. 139–145, 2005.
[52] Y. Feng, F. Sardei, and J. Kisslinger, "3D fluid modelling of the edge plasma by means of a Monte Carlo technique," *J. Nucl. Mater.*, vol. 266–269, pp. 812–818, 1999.
[53] D. Reiter, "The EIRENE Code User Manual," *http://www.eirene.de*. 2017.
[54] K. Ghoos, W. Dekeyser, G. Samaey, P. Börner, and M. Baelmans, "Accuracy and convergence of coupled finite-volume/Monte Carlo codes for plasma edge simulations of nuclear fusion reactors," *J. Comput. Phys.*, vol. 322, pp. 162–182, 2016.
[55] M. Baelmans, P. Börner, K. Ghoos, and G. Samaey, "Efficient code simulation strategies for B2-EIRENE," *Nucl. Mater. Energy*, vol. 12, pp. 858–863, 2017.
[56] K. Ghoos, P. Börner, W. Dekeyser, A. S. Kukushkin, and M. Baelmans, "Grid resolution study for B2-EIRENE simulation of partially detached," *Nucl. Fusion*, vol. 59, no. 2, p.

026001 (8pp), 2019.
[57] A. S. Kukushkin, H. D. Pacher, V. Kotov, G. W. Pacher, and D. Reiter, "Finalizing the ITER divertor design: The key role of SOLPS modeling," *Fusion Eng. Des.*, vol. 86, no. 12, pp. 2865–2873, 2011.
[58] D. REITER, C. MAY, D. COSTER, and R. SCHNEIDER, "Time Dependent Neutral Gas Transport in Tokamak Edge Plasmas," *J. Nucl. Mater.*, vol. 220–222, pp. 987–992, 1995.
[59] V. Kotov, "Particle conservation in numerical models of the tokamak plasma edge," *Phys. Plasmas*, vol. 24, no. 4, p. 042511 (6pp), 2017.
[60] S. I. Krasheninnikov, A. S. Kukushkin, V. I. Pistunovich, and V. A. Pozharov, "Self-sustained oscillations in the divertor plasma," *Nucl. Fusion*, vol. 27, no. 11, pp. 1805–1816, 1987.
[61] A. A. Pshenov, A. S. Kukushkin, and S. I. Krasheninnikov, "Energy balance in plasma detachment," *Nucl. Mater. Energy*, vol. 12, pp. 948–952, 2017.
[62] T. D. Rognlien *et al.*, "Comparison of 2D simulations of detached divertor plasmas with divertor Thomson measurements in the DIII-D tokamak," *Nucl. Mater. Energy*, vol. 12, pp. 44–50, 2017.
[63] C. Guillemaut *et al.*, "Influence of atomic physics on EDGE2D-EIRENE simulations of JET divertor detachment with carbon and beryllium/tungsten plasma-facing components," *Nucl. Fusion*, vol. 54, no. 9, p. 093012 (25pp), 2014.
[64] H. D. Pacher, A. S. Kukushkin, G. W. Pacher, V. Kotov, R. A. Pitts, and D. Reiter, "Impurity seeding in ITER DT plasmas in a carbon-free environment," *J. Nucl. Mater.*, vol. 463, pp. 591–595, 2015.
[65] B. Lipschultz, B. LaBombard, J. L. Terry, C. Boswell, and I. H. Hutchinson, "Divertor physics research on alcator C-Mod," *Fusion Sci. Technol.*, vol. 51, no. 3, pp. 369–389, 2007.
[66] B. Lipschultz *et al.*, "The role of particle sinks and sources in Alcator C-Mod detached divertor discharges," *Phys. Plasmas*, vol. 6, no. 5, pp. 1907–1916, 1999.
[67] F. Wising, D. A. Knoll, S. I. Krasheninnikov, T. D. Rognlien, and D. J. Sigmar, "Simulation of Detachment in ITER-Geometry Using the UEDGE Code and a Fluid Neutral Model," *Contrib. to Plasma Phys.*, vol. 36, no. 2–3, pp. 309–313, 1996.
[68] A. Kukushkin *et al.*, "2D modelling of radiating divertor regime for ITER," *J. Nucl. Mater.*, vol. 241–243, pp. 268–272, 1997.
[69] H. D. Pacher *et al.*, "Impurity seeding and scaling of edge parameters in ITER," *J. Nucl. Mater.*, vol. 390–391, pp. 259–262, 2009.
[70] M. Wischmeier *et al.*, "Assessment of edge modeling in support of ITER," *J. Nucl. Mater.*, vol. 415, no. 1 SUPPL, pp. S523–S529, 2011.
[71] A. V. Chankin, E. Delabie, G. Corrigan, C. F. Maggi, H. Meyer, and JET Contributors, "Possible influence of near SOL plasma on the H-mode power threshold," *Nucl. Mater. Energy*, vol. 12, pp. 273–277, 2017.
[72] S. Wiesen *et al.*, "On the role of finite grid extent in SOLPS-ITER edge plasma simulations for JET H-mode discharges with metallic wall," *Nucl. Mater. Energy*, vol. 17, pp. 174–181, 2018.
[73] A. E. Jaervinen *et al.*, "E × B Flux Driven Detachment Bifurcation in the DIII-D Tokamak," *Phys. Rev. Lett.*, vol. 121, no. 7, p. 75001, 2018.
[74] A. E. Jaervinen *et al.*, "Impact of drifts on divertor power exhaust in DIII-D," *Nucl. Mater. Energy*, vol. 19, pp. 230–238, 2019.

[75] B. LaBombard *et al.*, "Cross-field plasma transport and main-chamber recycling in diverted plasmas on Alcator C-Mod," *Nucl. Fusion*, vol. 40, no. 12, pp. 2041–2060, 2000.
[76] L. Aho-Mantila *et al.*, "Assessment of SOLPS5.0 divertor solutions with drifts and currents against L-mode experiments in ASDEX Upgrade and JET," *Plasma Phys. Control. Fusion*, vol. 59, no. 3, p. 035003 (18pp), 2017.
[77] S. Wiesen, W. Fundamenski, M. Wischmeier, M. Groth, S. Brezinsek, and V. Naulin, "Relevance of collisionality in the transport model assumptions for divertor detachment multi-fluid modelling on JET," *J. Nucl. Mater.*, vol. 415, no. 1 SUPPL, pp. S535–S539, 2011.
[78] A. V. Chankin *et al.*, "Comparison between measured divertor parameters in ASDEX Upgrade and SOLPS code solutions," *J. Nucl. Mater.*, vol. 363–365, no. 1–3, pp. 335–340, 2007.
[79] O. Czarny and G. Huysmans, "Bézier surfaces and finite elements for MHD simulations," *J. Comput. Phys.*, vol. 227, no. 16, pp. 7423–7445, 2008.
[80] V. Rozhansky, "Drifts, Currents, and Radial Electric Field in the Edge Plasma with Impact on Pedestal, Divertor Asymmetry and RMP Consequences," *Contrib. to Plasma Phys.*, vol. 54, no. 4–6, pp. 508–516, 2014.
[81] A. Loarte *et al.*, "Progress on the application of ELM control schemes to ITER scenarios from the non-active phase to DT operation," *Nucl. Fusion*, vol. 54, no. 3, p. 033007 (18pp), 2014.
[82] T. E. Evans *et al.*, "Suppression of Large Edge-Localized Modes in High-Confinement DIII-D Plasmas with a Stochastic Magnetic Boundary," *Phys. Rev. Lett.*, vol. 92, no. 23, p. 235003, 2004.
[83] W. Suttrop *et al.*, "First Observation of Edge Localized Modes Mitigation with Resonant and Nonresonant Magnetic Perturbations in ASDEX Upgrade," *Phys. Rev. Lett.*, vol. 106, no. 22, p. 225004, 2011.
[84] Y. Liang *et al.*, "Active Control of Type-I Edge-Localized Modes with n = 1 Perturbation Fields in the JET Tokamak," *Phys. Rev. Lett.*, vol. 98, no. 26, p. 265004, 2007.
[85] J.-W. Ahn *et al.*, "Effect of nonaxisymmetric magnetic perturbations on divertor heat and particle flux profiles in National Spherical Torus Experiment," *Phys. Plasmas*, vol. 18, no. 5, p. 56108, 2011.
[86] B. Lloyd *et al.*, "Overview of physics results from MAST," *Nucl. Fusion*, vol. 51, no. 9, p. 094013 (10pp), 2011.
[87] M. F. Heyn *et al.*, "Kinetic estimate of the shielding of resonant magnetic field perturbations by the plasma in DIII-D," *Nucl. Fusion*, vol. 48, no. 2, p. 024005, 2008.
[88] H. Stoschus *et al.*, "Rotation dependence of a phase delay between plasma edge electron density and temperature fields due to a fast rotating, resonant magnetic perturbation field," *Phys. Plasmas*, vol. 17, no. 6, p. 60702, 2010.
[89] I. Waters *et al.*, "Field aligned flows driven by neutral puffing at MAST," *Nucl. Fusion*, vol. 58, no. 6, p. 066002 (12pp), 2018.
[90] W. Suttrop, "The physics of large and small edge localized modes," *Plasma Phys. Control. Fusion*, vol. 42, no. 5A, pp. A1–A14, 2000.
[91] R. A. Pitts *et al.*, "Physics basis for the first ITER tungsten divertor," *Nucl. Mater. Energy*, vol. 20, no. 10, p. 100696, 2019.
[92] D. P. Coster, R. Schneider, J. Neuhauser, B. Braams, and D. Reiter, "Theory and Modelling of Time Dependent Phenomena in the Plasma Edge," *Contrib. to Plasma Phys.*,

vol. 36, no. 2–3, pp. 150–160, 1996.
[93] T. D. Rognlien and M. Shimada, “E × B-drift, current, and kinetic effects on divertor plasma profiles during ELMs,” *J. Nucl. Mater.*, vol. 313–316, no. SUPPL., pp. 1000–1004, 2003.
[94] D. P. Coster, “Whole device ELM simulations,” *J. Nucl. Mater.*, vol. 390–391, pp. 826–829, 2009.
[95] A. Y. Pigarov, S. I. Krasheninnikov, T. D. Rognlien, E. M. Hollmann, C. J. Lasnier, and E. Unterberg, “Multi-fluid transport code modeling of time-dependent recycling in ELMy H-mode,” *Phys. Plasmas*, vol. 21, no. 6, p. 062514 (14pp), 2014.
[96] S. J. P. Pamela *et al.*, “Recent progress in the quantitative validation of JOREK simulations of ELMs in JET,” *Nucl. Fusion*, vol. 57, no. 7, p. 076006 (11pp), 2017.
[97] M. Hoelzl *et al.*, “Insights into type-I edge localized modes and edge localized mode control from JOREK non-linear magneto-hydrodynamic simulations,” *Contrib. to Plasma Phys.*, vol. 58, pp. 518–528, 2018.
[98] S. J. P. Pamela *et al.*, “Resistive MHD simulation of edge-localized-modes for double-null discharges in the MAST device,” *Plasma Phys. Control. Fusion*, vol. 55, no. 9, p. 095001 (13pp) PLASMA, 2013.